Electron-trapping polycrystalline materials with negative electron affinity

KEITH P. McKENNA* AND ALEXANDER L. SHLUGER

Department of Physics and Astronomy and The London Centre for Nanotechnology, University College London, Gower Street, London, WC1E 6BT, UK

*e-mail: k.mckenna@ucl.ac.uk

Published online: 12 October 2008; doi:10.1038/nmat2289

The trapping of electrons by grain boundaries in semiconducting and insulating materials is important for a wide range of physical problems, for example, relating to: electroceramic materials[1] with applications as sensors, varistors[2] and fuel cells, reliability issues for solar cell[3] and semiconductor technologies[4,5] and electromagnetic seismic phenomena in the Earth's crust[6]. Surprisingly, considering their relevance for applications[7] and abundance in the environment, there have been few experimental or theoretical studies of the electron trapping properties of grain boundaries in highly ionic materials such as the alkaline earth metal oxides and alkali halides. Here we demonstrate, by first-principles calculations on MgO, LiF and NaCl, a qualitatively new type of electron trapping at grain boundaries. This trapping is associated with the negative electron affinity of these materials[8] and is unusual as the electron is confined in the empty space inside the dislocation cores.

Although it was proposed that grain boundaries can trap electrons many years ago[4], it is still a considerable experimental challenge to characterize the intrinsic electronic properties of grain boundaries in a way that is separated from that of various other defects and impurities; therefore, *ab initio* calculations of their electronic structure can bring important insights. The current understanding of electron trapping at grain boundaries, which is based mainly on density functional theory (DFT) studies of narrow to medium gap insulators[9,10], can be summarized in three main points: (1) grain boundaries that have the lowest energy (those thermodynamically favoured) reconstruct to leave no dangling bonds or low-coordinated atoms[11], (2) such reconstructed grain boundaries possess either very shallow electron traps (split from the bulk conduction band by tenths of an electronvolt) or no traps at all, (3) disordered intergranular phases[12], defects and impurities can be responsible for deep electron traps. However, it still remains unclear whether, in highly ionic wide-gap systems, defect-free, well-ordered grain boundaries can act as deep electron traps solely as a consequence of their intrinsic electronic structure. Taking the amount of speculations surrounding charge trapping at grain boundaries, answering this question is timely and important.

In general, polycrystalline materials contain a wide variety of interfaces between grains that can be influenced by numerous factors, such as growth conditions and thermal treatment. However, to develop an understanding of electron trapping in such complex systems, it is important to first focus on well-characterized interfaces. Here, we demonstrate that symmetric tilt grain boundaries, which for MgO have been studied extensively both experimentally[13,14] and theoretically[15–17], can trap electrons. This result is general for negative-electron-affinity (NEA) materials and important for MgO applications as secondary electron emitters in flat-panel displays[7], microwave dielectrics for wireless communications, gate dielectrics in transistors and tunnel barriers in magnetic random access memory devices[18]. MgO also has some advantage as a model system as its electronic properties are well understood in the bulk, at surfaces, in nanopowders and for numerous defects therein[19].

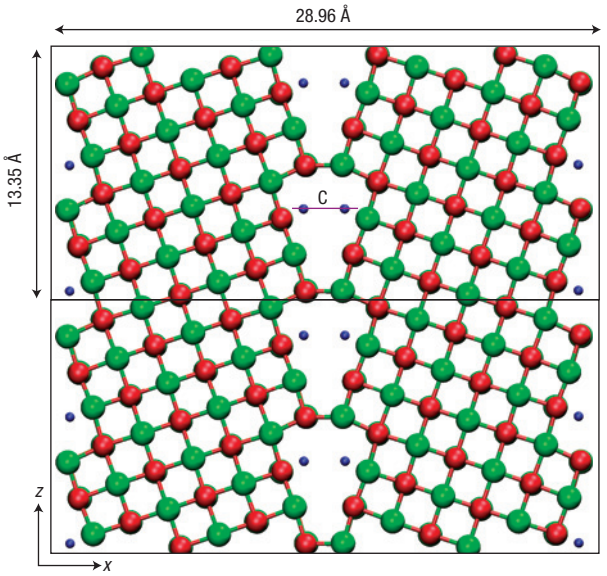

Figure 1 The periodic supercell (13.35 Å × 8.33 Å × 28.96 Å) used to model the (310)[001](36.8°) tilt grain boundary in MgO. (Similar cells are used for NaCl and LiF.) The positions of the Bader charges associated with an electron trapped inside the dislocation are indicated by blue points (see text and Fig. 2).

Our calculations show that in NEA materials, electrons can be trapped inside dislocations (which are a common feature of many grain boundaries, for example, see Fig. 1). In simple terms, this seemingly counter-intuitive result can be understood by taking into account that the average electrostatic potential in a dislocation core is, by symmetry, zero (vacuum level). As the conduction band in NEA materials is positioned above the vacuum level, electrons may become trapped if the kinetic energy associated with confining the electron in the dislocation is small compared with the magnitude of the NEA. We show below that this balance is favourable for MgO

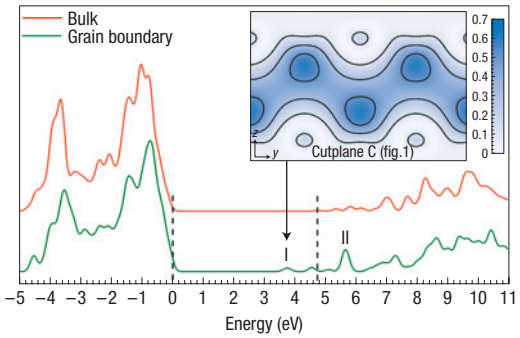

Figure 2 Comparison of the density of states of the grain-boundary supercell with bulk MgO. The dashed lines indicate the positions of the bulk valance-band maximum and conduction-band minimum. I and II label the electronic states associated with the grain boundary. The inset shows electron density isosurfaces through cutplane C identified in Fig. 1 for an electron in state I.

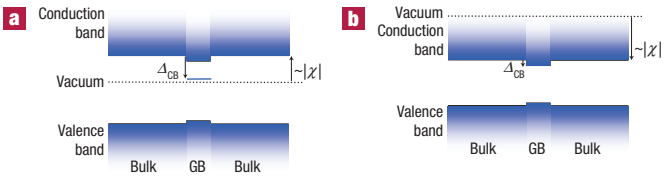

Figure 3 Qualitative differences in electron trapping at grain boundaries in positive- and negative-electron-affinity materials. a, For materials with NEA, the position of the bulk conduction-band minimum is about $|\chi|$ above the vacuum level. Therefore, the lowest unoccupied electron states at the grain boundary (GB) are free electron states confined inside the dislocation (blue line). **b**, For materials with positive electron affinity, similar states are not present in the bandgap; therefore only shallow, bulk-conduction- and valence-band-derived states are present.

and LiF and their unusual electronic properties can be probed with emerging techniques such as photon emission spectroscopy using scanning probes[20].

Grain-boundary models have been generated using a combination of atomistic and first-principles methods (see the Methods section). Electron trapping is investigated using both periodic DFT and an embedded cluster method. The latter has the advantages that the B3LYP hybrid density functional can be used, which predicts more accurate bandgaps for insulators, and also that no neutralizing background is needed for charged systems. This type of approach has been used successfully in previous studies of electron localization and good agreement with experiment has been obtained[21]. Figure 2 shows, for the (310)[001] (36.8°) tilt grain boundary (Fig. 1), the electronic density of states of the supercell together with a reference calculation for the bulk. To separate bulk and interface contributions to the electronic structure, the charge density associated with individual electronic states is calculated and their spatial distribution is analysed. States with density that is delocalized evenly throughout the grains are identified as bulk-like states, whereas those with increased amplitude near the grain boundary are identified as interface states. This analysis permits us to align the density of states curves in energy using the top of the bulk valence band as a common reference. We checked that this procedure yields a similar alignment as that obtained by comparing the average position of the core O 2*s* levels. Whereas there is only a small splitting (<0.1 eV) of occupied interface states from the top of the valence band, two sets of unoccupied states, labelled I and II in Fig. 2, are more significantly split from the bulk conduction band, which starts just below 5 eV. Using the embedded cluster method, calculated bandgaps are increased but the splitting of interface states is qualitatively similar (see the Methods section). We mainly present results from the periodic calculations, as this provides a more natural description of the delocalized interface states.

The interface states labelled I are located 1 eV below the bulk conduction-band minimum, and therefore present a trap for conduction-band electrons. To understand the nature of the electron trapping, an electron is added to the system and the supercell geometry is optimized. A Bader analysis of the charge density shows that the electron is primarily (about 80%) located inside the dislocation core. The remaining 20% is attributed to nearby anions and this density is strongly polarized towards the centre of the core. The blue points in Fig. 1 show the locations of the associated Bader charges, which follow the centre of mass of the electron distribution. Electron density isosurfaces for a cutplane through the dislocation core are shown in the inset of Fig. 2. The confined electron snakes its way down the centre of the dislocation cores, following the weakly attractive electrostatic potential of Mg^{2+} ions on the internal surfaces. The band dispersion of this electronic state along the core axis has been calculated and it defines an electron effective mass very close to unity. The grain boundary also introduces resonant states in the bulk conduction band (labelled II in Fig. 2). The higher energy of these states is explained by their association with the more confined part of the dislocation core. The electronic structure and electron trapping properties of grain boundaries in NaCl and LiF are very similar to that for MgO. In all cases the splitting of states from the valence band is less than 0.1 eV; however, the splitting of states from the conduction band (Δ_{CB}) varies considerably. Deep electron traps are found for MgO and LiF grain boundaries, whereas a relatively shallow trap is found for NaCl (the results are summarized in Table 1).

Interface states associated with grain boundaries are usually associated with under-coordinated atoms at the boundary and structural relaxation. However, here we find interface states concentrated inside dislocation cores, which can trap electrons. We have also considered different tilt grain boundaries of the form (x10)[001] (where x is a positive integer) and found their electronic properties to be qualitatively similar. Although this electron trapping seems analogous to the localization of electrons inside oxygen vacancies or at surface irregularities, such as steps and divacancies (for example, see ref. 20 and refs within), there are qualitative differences. In the case of colour centres in MgO, it is the Madelung potential that energetically favours the localization of electrons at the vacancy site, and associated with these defects are deep electronic levels positioned near the middle of the MgO bandgap. At surfaces, electron trapping is connected with the electron affinity of low-coordinated cations, which are not present in the low-energy boundaries we consider.

Our first-principles calculations demonstrate that electron trapping is favourable. A simpler calculation below, based on experimental data, shows that this result is actually expected. To determine whether an electron can be trapped inside a dislocation core, the confinement energy should be compared with the electron affinity (χ). Using a particle-in-a-box model and taking the average diameter of the dislocation as 4.5 Å and the barrier height as 1 eV (ref. 22) ($|\chi|$), a kinetic energy of 0.5 eV is obtained. This is smaller than $|\chi|$, demonstrating trapping is favoured, but the potential well is deepened further in reality by the short-range positive electrostatic potential that surrounds cations and by polarization of surrounding ions. A previous theoretical calculation[8] has shown that image states on the MgO surface are bound by 0.5 eV,

Table 1 Summary of results for the (310)[001] tilt grain boundary in NaCl, MgO and LiF. E_f is the formation energy of the boundary per unit area, E_g^{bulk} is the calculated bulk bandgap, Δ_{CB} is the splitting of states from the conduction band and χ is the experimentally determined electron affinity.

	E_f ($J\,m^{-2}$)	E_g^{bulk} (eV)	Δ_{CB} (eV)	χ (eV)
NaCl	0.2	5.1	0.3	−0.1 (ref. 29)
MgO	1.3	4.9	1.0	−1.0 (ref. 22)
LiF	0.4	9.8	1.9	−3.1 (ref. 30)

indicating that the interplay between confinement and polarization in these systems is highly favourable. Here, we find that the splitting of interface states from the bulk conduction band is given approximately by $|\chi|$ (Fig. 3a); therefore, deep electron traps can be present even in well-ordered grain boundaries if $|\chi|$ is large. In contrast, for materials with positive electron affinity, there is only a small splitting of states from the bulk conduction and valence band (Fig. 3b). This idea is supported by the correlation between Δ_{CB} and the electron affinity shown in Table 1. LiF has the largest NEA and the largest splitting of states from the bulk conduction band, whereas NaCl has almost zero NEA and a very small splitting. Therefore, this type of electron trapping should be important not only for MgO, but for other NEA materials, such as boron nitride and alumina. As preferential hole trapping at grain boundaries is not favoured, the effect provides a mechanism for the separation of electrons and holes, for example, under irradiation.

The fundamental properties of such a confined electron gas, which has some similarities with effects observed at polar oxides interfaces[23], should be possible to study experimentally using a wide range of techniques. For example, internal electric fields generated under irradiation can influence the electronic state of impurities and defects, which can be probed by photospectroscopy[6] methods. Thin insulating films on metal substrates accommodate strain by dislocations, which can be individually addressed by scanning probe techniques such as scanning tunnelling spectroscopy or Kelvin probe[24,25]. The stimulation of photon emission by electron injection from a scanning tunnelling microscopy tip has recently been demonstrated on MgO films[20]. The ability to map photon emission with nanometre precision provides an opportunity to directly study the electronic and optical properties of individual dislocations. The presence of electronic states below the bulk conduction band should also be manifested in reduced barrier heights measured by four-point-probe transport measurements on high-quality bi-crystals[26] and polycrystalline films.

It is interesting to consider if the properties of these grain boundaries could be developed into a new method of characterization. In this respect, it should be noted that in many ways grain boundaries in NEA materials have similar properties to their surfaces. For example, we have calculated the optical spectra of the (310) grain-boundary dislocation using time-dependent DFT. The dominant excitation occurs at 6 eV, which overlaps with the absorption band that is normally assigned to (100) surfaces[8]. Therefore, the intensity of this band provides a measure of the concentration of grain boundaries in the system. We have also calculated the properties of colour-centre defects at grain boundaries (for example, see ref. 20 for a description of the method). Again, we find the properties of these defects are very similar to their surface analogues, so experimental methods that probe them, such as electron paramagnetic resonance, may provide an indirect measure of the concentration of grain boundaries.

These effects also have broader relevance to radiation-induced charging, luminescence and dielectric breakdown in polycrystalline metal-oxide materials. In this context, we have calculated the properties of a HfO_2 grain boundary. In this case, grain-boundary-related electronic states are split by 0.4 eV from both the conduction and valence bands; therefore, the segregation of both electrons and holes to HfO_2 grain boundaries is favoured. These electronic states are associated with the ions at the interface, rather than the space between the grains. This is expected because unlike MgO, HfO_2 has a positive electron affinity.

In summary, our first-principles calculations of the electronic structure of grain boundaries in MgO, NaCl and LiF show that they can act as a trap for conduction-band electrons. Our investigation reveals a novel form of electron trapping associated with one-dimensional electronic states that are localized inside dislocation cores. In addition to such effects being important for many applied physics problems, purposely filling dislocations with electrons (electrically or optically, for example) opens up interesting possibilities for fundamental studies of confined electron systems.

METHODS

To calculate the electronic properties of pristine and defective grain boundaries, we have developed a hierarchical approach using both atomistic models and DFT methods. We calculate the structure and formation energies of grain boundaries using a polarizable shell-model potential for MgO and the METADISE code (for example, see ref. 17). The structure of the interface is optimized with respect to lateral translations, intergrain dilations and also the addition and removal of ions at the interface. From this structure, a three-dimensional periodic supercell is constructed (Fig. 1). The supercell used for the calculations has the grain boundaries separated by about 15 Å, which is sufficient to ensure the electrostatic and elastic interaction between them is negligible. To calculate electronic properties, we use periodic DFT using the projector-augmented wave method and the PW91 functional[27] as implemented in the Vienna *ab initio* Simulation Package code[28]. The gamma point is sampled with a plane-wave cutoff of 400 eV and the atomic coordinates and cell dimensions are optimized to within a force tolerance of 0.01 eV $Å^{-1}$. DFT tends to underestimate the bandgap, E_g, of ionic insulators; therefore, to check the reliability of our results, we have also carried out calculations using the B3LYP hybrid-density functional within an embedded cluster method[19]. For MgO, we obtain the following results: $E_g = 4.9$ eV, $\Delta_{CB} = 1.0$ eV (generalized-gradient-approximation DFT); $E_g = 7.9$ eV, $\Delta_{CB} = 1.5$ eV (B3LYP with 20% Hartree–Fock exchange); and $E_g = 9.3$ eV, $\Delta_{CB} = 1.8$ eV (B3LYP with 32.5% Hartree–Fock exchange). The electronic state that is confined inside the dislocation core is qualitatively similar in all cases. Optical absorption spectra have also been calculated using time-dependent DFT and the embedded cluster method.

Received 21 January 2008; accepted 11 September 2008; published 12 October 2008.

References

1. Waser, R. & Hagenbeck, R. Grain boundaries in dielectric and mixed-conducting ceramics. *Acta Mater.* **48**, 797–825 (2000).
2. Clarke, D. R. Varistor ceramics. *J. Am. Ceram. Soc.* **82**, 485–502 (1999).
3. Yan, Y., Noufi, R. & Al-Jassim, M. M. Grain-boundary physics in polycrystalline $CuInSe_2$ revisited: Experiment and theory. *Phys. Rev. Lett.* **96**, 205501 (2006).
4. Seto, J. Y. W. The electrical properties of polycrystalline silicon films. *J. Appl. Phys.* **46**, 5247–5254 (1975).
5. Walker, P. M., Mizuta, H., Uno, S., Furuta, Y. & Hasko, D. G. Improved off-current and subthreshold slope in aggressively scaled poly-Si TFTs with a single grain boundary in the channel. *Electron Devices IEEE Trans.* **51**, 212–219 (2004).
6. Takeuchi, A., Nagahamab, H. & Hashimotoa, T. Surface electrification of rocks and charge trapping centers. *Phys. Chem. Earth A/B/C* **29**, 359–366 (2004).
7. Vink, T. J., Balkenende, A. R., Verbeek, R. G. F. A., van Hal, H. A. M. & de Zwart, S. T. Materials with a high secondary-electron yield for use in plasma displays. *Appl. Phys. Lett.* **80**, 2216–2218 (2002).
8. Rohlfing, M., Wang, N.-P., Krüger, P. & Pollmann, J. Image states and excitons at insulator surfaces with negative electron affinity. *Phys. Rev. Lett.* **91**, 256802 (2003).
9. Kohyama, M. Computational studies of grain boundaries in covalent materials. *Modelling Simul. Mater. Sci. Eng.* **10**, R31 (2002).
10. Dawson, I. *et al.* First-principles study of a tilt grain boundary in rutile. *Phys. Rev. B* **54**, 13727–13733 (1996).
11. von Alfthan, S., Haynes, P. D., Kaski, K. & Sutton, A. P. Are the structures of twist grain boundaries in silicon ordered at 0 K? *Phys. Rev. Lett.* **96**, 055505 (2006).
12. Clarke, D. R. Grain boundaries in polycrystalline ceramics. *Annu. Rev. Mater. Sci.* **17**, 57–74 (1987).
13. Kizuka, T., Iijima, M. & Tanaka, N. Atomic process of electron-irradiation-induced grain boundary migration in a MgO tilt boundary. *Phil. Mag. A* **77**, 413–422 (1998).
14. Yan, Y. *et al.* Impurity-induced structural transformation of a MgO grain boundary. *Phys. Rev. Lett.* **81**, 3675–3678 (1998).
15. Duffy, D. M. Grain boundaries in ionic crystals. *J. Phys. C* **19**, 4393–4412 (1986).

16. Watson, G. W., Kelsey, E. T., de Leeuw, N. H., Harris, D. J. & Parker, S. C. Atomistic simulation of dislocations, surfaces and interfaces in MgO. *J. Chem. Soc. Faraday Trans.* **92**, 433–438 (1996).
17. Harding, J. H., Harris, D. J. & Parker, S. C. Computer simulation of general grain boundaries in rocksalt oxides. *Phys. Rev. B* **60**, 2740–2746 (1999).
18. Parkin, S. S. P. *et al.* Giant tunnelling magnetoresistance at room temperature with MgO (100) tunnel barriers. *Nature Mater.* **3**, 862–867 (2004).
19. McKenna, K. P., Sushko, P. V. & Shluger, A. L. Inside powders: A theoretical model of interfaces between MgO nanocrystallites. *J. Am. Chem. Soc.* **129**, 8600–8608 (2007).
20. Benia, H.-M., Myrach, P. & Nilius, N. Photon emission spectroscopy of thin MgO films with the STM: From a tip-mediated to an intrinsic emission characteristic. *New J. Phys.* **10**, 013010 (2008).
21. Sushko, P. V., Shluger, A. L., Hirano, M. & Hosono, H. From insulator to electride: A theoretical model of nanoporous oxide $12CaO{\cdot}7Al_2O_3$. *J. Am. Chem. Soc.* **129**, 942–951 (2007).
22. Stevenson, J. R. & Hensley, E. B. Thermionic and photoelectric emission from magnesium oxide. *J. Appl. Phys.* **32**, 166 (1961).
23. Tsukazaki, A. *et al.* Quantum Hall effect in polar oxide heterostructures. *Science* **315**, 1388–1391 (2007).
24. Mather, P. G., Read, J. C. & Buhrman, R. A. Disorder, defects, and band gaps in ultrathin (001) MgO tunnel barrier layers. *Phys. Rev. B* **73**, 205412 (2006).
25. Barth, C. & Henry, C. R. Kelvin probe force microscopy on surfaces of UHV cleaved ionic crystals. *Nanotechnology* **17**, S155S161 (2006).
26. Sato, Y. *et al.* Atomic and electronic structure of symmetric tilt grain boundary in ZnO bicrystal with linear current–voltage characteristic. *J. Mater. Sci.* **40**, 3059–3066 (2005).
27. Perdew, J. P. & Wang, Y. Accurate and simple analytic representation of the electron–gas correlation energy. *Phys. Rev. B* **45**, 13244–13249 (1992).
28. Kresse, G. & Joubert, J. From ultrasoft pseudopotentials to the projector augmented-wave method. *Phys. Rev. B* **59**, 1758–1775 (1999).
29. Eby, J. E., Teegarden, K. J. & Dutton, D. B. Ultraviolet absorption of alkali halides. *Phys. Rev.* **116**, 1099–1105 (1959).
30. Lapiano-Smith, D. A., Eklund, E. A., Himpsel, F. J. & Terminello, L. J. Epitaxy of LiF on Ge(100). *Appl. Phys. Lett.* **59**, 2174–2176 (1991).

Acknowledgements

Computer time on HPCx was provided through EPSRC grant EP/D504872/1. We acknowledge useful discussions with P. Sushko, M. Stoneham and G. Besurker. K.P.M. is supported by EPSRC grant GR/S80080/01.

Author information

Reprints and permissions information is available online at http://npg.nature.com/reprintsandpermissions. Correspondence and requests for materials should be addressed to K.P.M.